














Ultrafast control of the crystal structure in a topological charge-density-wave material

Takeshi Suzuki ^{1,*}, Yuya Kubota ², Natsuki Mitsuishi ³, Shunsuke Akatsuka,⁴ Jumpei Koga,⁴ Masato Sakano ⁴, Satoru Masubuchi,⁵ Yoshikazu Tanaka,² Tadashi Togashi ^{2,6}, Hiroyuki Ohsumi ², Kenji Tamasaku ², Makina Yabashi ^{2,6}, Hidefumi Takahashi ^{7,8}, Shintaro Ishiwata ^{7,8}, Tomoki Machida ⁵, Iwao Matsuda ¹, Kyoko Ishizaka,^{3,4} and Koza Okazaki ^{1,†}

¹*Institute for Solid State Physics, The University of Tokyo, Kashiwa, Chiba 277-8581, Japan*

²*RIKEN SPring-8 Center, 1-1-1 Kouto, Sayo, Hyogo 679-5148, Japan*

³*RIKEN Center for Emergent Matter Science (CEMS), Wako 351-0198, Japan*

⁴*Quantum-Phase Electronics Center and Department of Applied Physics, The University of Tokyo, Tokyo 113-8656, Japan*

⁵*Institute of Industrial Science, The University of Tokyo, Meguro-ku, Tokyo 153-8505, Japan*

⁶*Japan Synchrotron Radiation Research Institute (JASRI), 1-1-1 Kouto, Sayo, Hyogo 679-5198, Japan*

⁷*Division of Materials Physics and Center for Spintronics Research Network (CSR/N), Graduate School of Engineering Science, Osaka University, Toyonaka, Osaka 560-8531, Japan*

⁸*Spintronics Research Network Division, Institute for Open and Transdisciplinary Research Initiatives, Osaka University, Yamadaoka 2-1, Suita, Osaka 565-0871, Japan*



(Received 17 May 2023; revised 18 September 2023; accepted 1 November 2023; published 22 November 2023)

The optical control of crystal structures is a promising route to change physical properties including the topological nature of a targeting material. Time-resolved x-ray diffraction measurements using an x-ray free-electron laser are performed to study the ultrafast lattice dynamics of VTe_2 , which is known to possess a unique charge-density-wave (CDW) ordering coupled to the topological surface states as a first-order phase transition. A significant oscillation of the CDW amplitude mode is observed at a superlattice reflection as well as Bragg reflections. The frequency of the oscillation is independent of the fluence of the pumping laser, which is prominent in the CDW ordering of the first-order phase transition. Furthermore, the timescale of the photoinduced $1T''$ to $1T$ phase transition is not equal to the half period of the CDW amplitude mode, which is typically the case for Peierls insulators.

DOI: [10.1103/PhysRevB.108.184305](https://doi.org/10.1103/PhysRevB.108.184305)

I. INTRODUCTION

Engineering crystal structures is one of the direct ways to change the electronic, optical, and mechanical properties in solid state materials. Many techniques of structural control have been developed including strain [1], nanostructuring [2], heterostructure layer stacking [3], and twistrionics [4,5]. While these approaches are very powerful, investigations are limited to equilibrium states, where all the degrees of freedom are thermally balanced. On the other hand, a combination of photoexcitation by ultrafast pulse lasers and various probing techniques has enabled us to study nonequilibrium states, where a specific subsystem is selectively excited, by which many exotic phenomena have been reported [6]. Ultrafast optical pulses have also served as powerful tools to engineer crystal structures, by which a variety of phases, including superconductivity [7,8], ferroelectricity [9,10], and magnetism [11], have been found to emerge.

Recently, controlling the topological properties of a material by light has attracted enormous interest because a topological insulator has robust metallic surface states against impurities or disorder [12,13], which is preferable for optical switching. While many approaches to ultrafast

topological control have been demonstrated by Floquet engineering [14–17], controlling crystal structures with light has also been employed to manipulate topological properties [18,19]. This methodology is also applicable to charge-density-wave (CDW) materials having topological properties. A great advantage of using CDW materials is the feasibility of flexibly tuning their properties by external stimuli such as physical [20,21] or chemical pressure [22,23], and electric [24–26] or magnetic fields [27].

For the optical control of CDW materials, many studies have been reported mainly in the context of collective-mode excitations or photoinduced phase transitions. Since a CDW phase is a coupled phase between the charge and lattice, multiple ultrafast probing techniques have been employed to track different degrees of freedom, including optical pump-probe spectroscopy [28–30], time- and angle-resolved photoemission spectroscopy (ARPES) [31–34], ultrafast electron diffraction (UED) [35–38], and time-resolved x-ray diffraction (TRXRD) [39–43]. These reports have highlighted second-order CDW phase transition systems except for $1T$ - TaS_2 . On the other hand, a specific phase is preserved against the external turbulence within the threshold in a first-order phase transition. Such a *robustness* of the phase is a great advantage over a second-order phase transition, especially for the application of ultrafast devices such as an optical switch or memory medium. In terms of fundamental physics, the kinetics of first-order photoinduced phase transitions shows many

*takeshi.suzuki@issp.u-tokyo.ac.jp

†okazaki@issp.u-tokyo.ac.jp

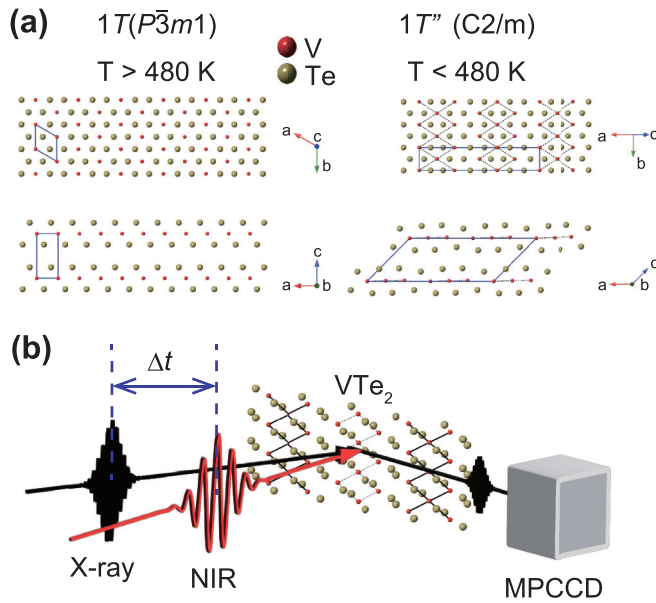


FIG. 1. (a) Crystal structure of VTe_2 . Above the phase transition temperature of 480 K, VTe_2 displays a $1T$ ($P\bar{3}m1$) structure while below 480 K it shows a $1T''$ ($C2/m$) structure. The double-zigzag bonds of the V atoms in the $1T''$ phase are shown as dashed black lines and a unit cell for each phase is shown as a solid blue box. (b) Schematic illustration of the time-resolved x-ray diffraction measurement. The delay time between the near-infrared (NIR) pump and the hard x-ray probe is shown as Δt . The diffracted signal is detected by a multiphoton charge-coupled device (MPCCD).

attractive phenomena such as nucleation [44] or percolative dynamics [45]. Thus, it is highly desired to study in detail the dynamical features of a first-order photoinduced CDW phase transition system having intriguing profiles.

In this paper, we report ultrafast lattice dynamics in VTe_2 , which has a first-order CDW phase transition and the topological surface states coupled to the CDW phase, by performing the measurements of TRXRD using an x-ray free-electron laser (XFEL). We directly observe the CDW amplitude mode in VTe_2 as a significant temporal oscillation, 1.5 THz in frequency, of a superlattice reflection. We further study CDW melting dynamics by the pump-fluence-dependent measurements. Through the fitting analysis, we successfully reveal the distinctive features of a first-order CDW phase transition. They are quite different from many other CDW materials of second-order phase transitions. Our findings provide detailed guidelines for the crystal structure control of first-order CDW materials and an important step towards the manipulation of topological surface states.

II. EXPERIMENTAL METHODS

Figure 1(a) shows the crystal structure of VTe_2 in the $1T$ ($P\bar{3}m1$, No. 164 trigonal) metallic and $1T''$ ($C2/m$, No. 12 monoclinic) CDW phases, where a unit cell for each phase is shown as a solid blue box. With lowering temperature, VTe_2 displays the CDW phase transition at 480 K, accompanied by the formation of a $3 \times 1 \times 3$ superstructure characterized by the double-zigzag chain structure for the V atoms along the b direction, shown as dashed black lines in Fig. 1(a) [46].

One of the most striking signatures is the significantly large contraction of the V-V bonds ($\sim 9.1\%$ [46]), which is larger than the Ta-Ta bonds in the well-known CDW material $1T$ - TaS_2 ($\sim 7.0\%$ [47]). The hysteresis of resistivity in VTe_2 [48] also confirms that this CDW transition in VTe_2 is of first order. Furthermore, a recent study of angle-resolved photoemission spectroscopy revealed an intimate relationship between the topological surface states and CDW order [49], where two of three Dirac surface states at the boundary of the first Brillouin zone in the $1T$ metallic phase were found to disappear in the $1T''$ CDW phase. For the CDW melting dynamics, UED measurements were performed to directly observe the lattice dynamics and acoustic phonons of VTe_2 [50,51]. However, due to the limitation of the time resolution of ~ 2 ps, the initial dynamics of the CDW melting has remained uncovered. The optical pump-probe measurements with a sufficient time resolution were performed to observe multiple coherent phonons [52,53] while direct insight into the lattice dynamics is still missing.

To directly track the lattice dynamics with a high temporal resolution, we perform the measurements of TRXRD at BL3 of the XFEL facility, SPring-8 Angstrom Compact free-electron LASer (SACLA) [54] as schematically shown in Fig. 1(b). The details of the experimental setup and bulk sample preparation are given in the Supplemental Material [55]. To minimize the penetration-length mismatch between the NIR pump and x-ray probe (23 nm [52] and ~ 10 μm , respectively, for VTe_2), we prepared the samples with a thickness of ~ 40 nm using mechanical exfoliation by transparent adhesive tape and dry transfer onto a Si_3N_4 membrane [55]. The thickness of the sample was measured by both atomic force microscopy and acoustic wave measurements [55]. The integrated intensity of the diffracted image I_{hkl} is given by the structure factor F_{hkl} as expressed by $I_{hkl} \propto |F_{hkl}|^2$, and the structure factor is determined by atomic positions in a unit cell as

$$F_{hkl} = \sum_n f_n \exp(i\mathbf{G}_{hkl} \cdot \mathbf{r}_n), \quad (1)$$

where hkl is the Bragg reflection index, f_n is the atomic form factor of the n th atom, \mathbf{G}_{hkl} is the reciprocal vector, and \mathbf{r}_n is the atomic position of the n th atom. For the Bragg reflection indices in the main text, we use a practical monoclinic lattice [51,55]. The changes in the diffraction angle of Bragg reflections reflect the changes in the lattice constants [62] while the changes in the diffraction intensity reflect the atomic displacements inside the unit cell.

III. RESULTS AND DISCUSSIONS

Figure 2(a) shows the time dependence of the superlattice reflection intensity $I_{\frac{2}{3}0\frac{1}{3}}$ obtained with a low pump fluence of 0.8 mJ/cm^2 . One can clearly see a significant oscillation. The superlattice reflection only manifests in the $1T''$ phase and is structurally forbidden in the $1T$ phase, and thus its structure factor is determined by the extent of the Peierls distortion x . More specifically, the leading term of $F_{\frac{2}{3}0\frac{1}{3}}$ is proportional to x [63], and that of $I_{\frac{2}{3}0\frac{1}{3}}$ is proportional to $|x|^2$. Therefore, the modulation of the superlattice reflection

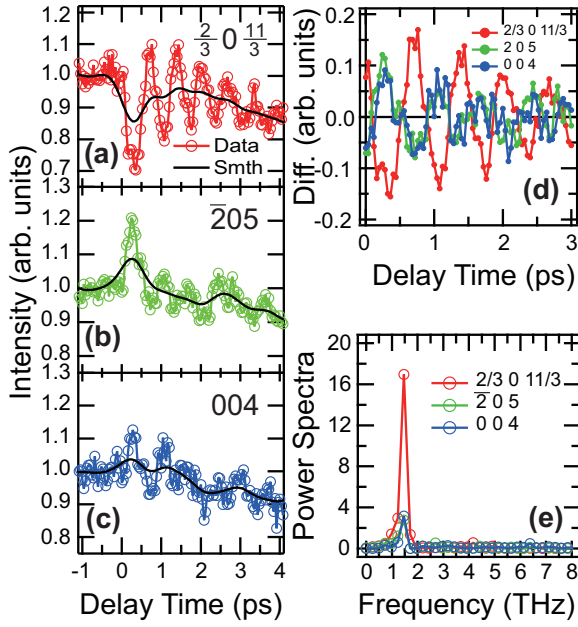


FIG. 2. (a)–(c) Time-dependent $I_{\frac{2}{3}0\frac{11}{3}}$, I_{205} , and I_{004} , at pump fluences of 0.8, 1.2, and 1.0 mJ/cm^2 , respectively. The data are shown as marks and the smoothing lines (smth) are shown as solid black lines. (d) Oscillatory components of (a)–(c) deduced by subtracting smoothing lines from data. (e) Power spectra of the oscillatory components (d).

intensity can be attributed to the excitation of the CDW amplitude mode. Several previous studies using TRXRD on other CDW materials also linked the oscillation of superlattice reflections to the CDW amplitude modes [40,42,43]. To further confirm this assignment, we also measure the Bragg reflection intensities of I_{205} and I_{004} as shown in Figs. 2(b) and 2(c). For both reflections, oscillations can be recognized. To deduce the oscillatory components, we subtract the backgrounds given by the smoothed lines shown as the solid black lines in Figs. 2(a)–2(c). The subtracted data are shown in Fig. 2(d). Interestingly, the oscillation phases of the Bragg reflections are opposite to that of the superlattice reflection, i.e., while the $I_{\frac{2}{3}0\frac{11}{3}}$ decreases in the first quarter cycle, the I_{205} and I_{004} increase. Fourier transforms are performed for the subtracted data and the power spectra are shown in Fig. 2(e). One can find a single-peak structure at 1.5 THz in all the diffraction intensities. This frequency corresponds to f_{AM} in Eq. (3) discussed later.

To understand the opposite oscillation phase between the superlattice and Bragg reflections, we consider the origin of the intensity modulation of the Bragg reflections in terms of the structure factors. While it is assumed that the photoinduced phase cannot be simply expressed using the structures of $1T$ and $1T''$ phases, here we approximate the structure factor in the photoinduced phase as the superposition of F_{1T} and $F_{1T''}$. F_{205} and F_{004} are calculated from Eq. (1) for both the $1T$ and $1T''$ phases [55], and shown in Table I. Both $|F_{205}|$ and $|F_{004}|$ for the $1T$ phase are larger than those for the $1T''$ phase. This is consistent with the increasing behavior in the first quarter cycle and further supports the assignment of the CDW amplitude mode. We note that the 1.5 THz coherent

TABLE I. Structure factors of VTe_2 for $1T$ and $1T''$ phases.

	$F_{1T''}$	F_{1T}	$I_{1T}/I_{1T''}$
$\bar{2}05$	$282 + 39i$	$410 + 58i$	2.12
004	$363 + 45i$	$516 + 65i$	2.02

phonon was also confirmed by a previous optical pump-probe measurement [52].

In order to investigate the CDW melting dynamics in VTe_2 , we perform the measurements with a higher pump fluence. Figure 3(a) shows the fluence-dependent dynamics of $I_{\frac{2}{3}0\frac{11}{3}}$. While the CDW amplitude mode is clearly observed at low fluences, it becomes strikingly suppressed with increasing fluence. Furthermore, the intensity drops immediately after the pump excitation increases, to one-tenth of the initial value at the highest fluence, which corresponds to the modulation from a structure of the $1T''$ CDW phase to that close to the $1T$ metallic phase. Figure 3(b) schematically shows these observations in terms of lattice dynamics in real space. Under low fluences, the V atoms smoothly oscillate with small displacements to new stable positions, the same mechanism as the displacive excitation of coherent phonons (DECP) [64]. Under high fluences, on the other hand, the V atoms are largely displaced from their original positions while the damping is strong enough to prevent multicycle oscillations. At a large delay time of 3–4 ps, the intensity decreases with pump

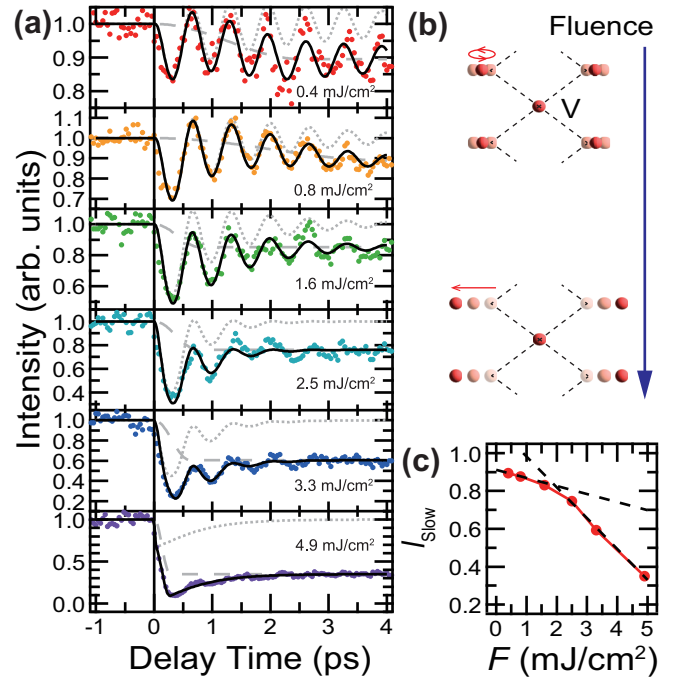


FIG. 3. (a) Fluence-dependent dynamics of $I_{\frac{2}{3}0\frac{11}{3}}$. The fluences are indicated in each panel. The data are shown as markers and the total fits are shown as solid black lines. The fits are composed of $I_1(t)$ and $I_2(t)$, and they are shown as dashed gray and dotted gray lines, respectively. (b) Schematic illustration of the fluence-dependent CDW amplitude mode. (c) Averaged intensity at $\Delta t = 3-4$ ps, I_{Slow} , as a function of pump fluence F .

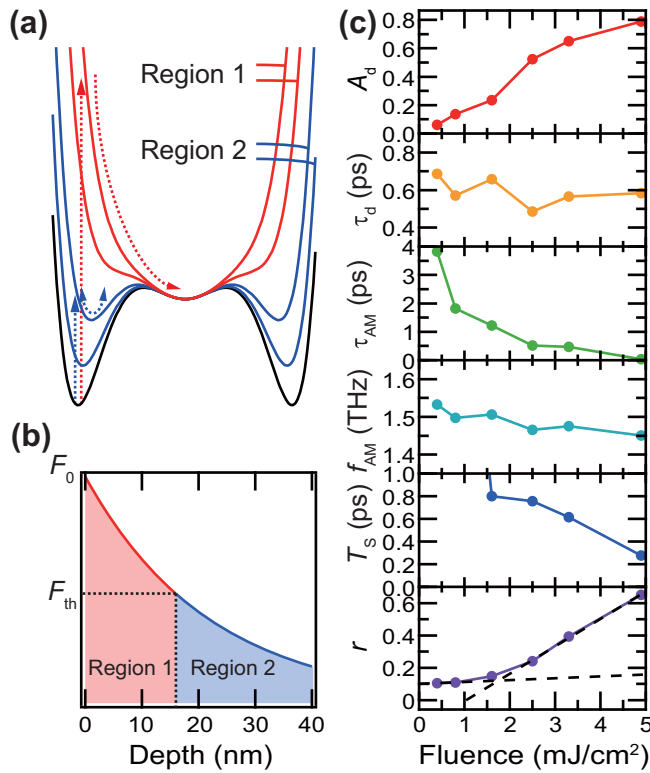


FIG. 4. (a) Schematic picture of the energy potential and dynamics after photoexcitation in a first-order phase transition system. (b) Schematic illustration of the two-component distribution of the excitation along the depth direction. Regions 1 and 2 are the photoinduced metallic and CDW phases, respectively. (c) Summary of the fitting parameters as a function of pump fluence. The dashed lines are linear fits at low and high fluences.

fluence and does not recover to the original value. To show this behavior more clearly, we plot the corresponding values of the intensity as a function of pump fluence in Fig. 3(c). Here, I_{Slow} represents the averaged intensity during $\Delta t = 3\text{--}4$ ps. I_{Slow} decreases almost monotonically but slightly nonlinearly with pump fluence. To highlight this behavior, we linearly fit the data at the low ($< 1.5 \text{ mJ}/\text{cm}^2$) and high fluences ($\geq 2.5 \text{ mJ}/\text{cm}^2$) and these lines are found to cross each other at $1.9 \text{ mJ}/\text{cm}^2$. This value implies the threshold fluence of the CDW melting, and we intensively discuss the melting dynamics in the following.

As we mentioned, VTe_2 is a first-order CDW phase transition material as $1T\text{-TaS}_2$. The photoinduced phase transition, then, can be pictured by the Landau potential for the first-order phase transition shown in Fig. 4(a) [65]. Furthermore, the boundary between the $1T''$ CDW and $1T$ metallic phases is rather well separated by a so-called phase boundary, so thus we assume the superlattice reflections during the photoinduced phase transition can be approximated as two spatially separate components. Due to the attenuation of pump excitation, the photoinduced $1T$ phase is triggered in a shallower region from the surface (region 1) while the CDW phase remains in a deeper region from the surface (region 2). Figure 4(b) schematically shows this situation, where the incident pump fluence at the surface is denoted as F_0 and the threshold pump fluence for the CDW melting is denoted as

F_{th} , which is estimated to be $1.9 \text{ mJ}/\text{cm}^2$ from Fig. 3(c). This value nearly agrees with the previous study of $1.21 \text{ mJ}/\text{cm}^2$ [52]. In general, photoinduced states are not necessarily the same as the equilibrium states as shown in previous studies [66]. These states are sometimes called “hidden” states. However, our data obtained by time-resolved x-ray diffraction measurements can be mostly explained by the superposition of equilibrium states. The residuals of the fits are due to the limitation of our treatments.

We use the phenomenological two-component model composed of $I_1(t)$ and $I_2(t)$ for the intensity of superlattice reflections from regions 1 and 2, respectively, shown below, in the same manner as previous work on $1T\text{-TaS}_2$ [41],

$$I_1(t) = \frac{1}{2} \left(1 + \cos \frac{\pi t}{T_s} \right), \quad 0 < t < T_s, \quad (2)$$

$$I_2(t) = (1 + A_d [\cos(2\pi f_{AM} t) e^{-t/\tau_{AM}} - e^{-t/\tau_d}])^2. \quad (3)$$

$I_1(t)$ is a sigmoid-shaped function, where T_s is the CDW melting time. $I_2(t)$ stands for the square of the atomic displacement for DECP dynamics. A_d , f_{AM} , and τ_{AM} are the amplitude, frequency, and decay constant for the CDW amplitude modes, respectively, τ_d is the relaxation time back to the initial potential for region 2. We fit our experimental data by $I_{\text{Total}}(t) = rI_1(t) + (1-r)I_2(t)$, where r is the volume fraction of region 1.

The total fitting results are shown as solid black lines in Fig. 3(a), where $I_1(t)$ and $I_2(t)$ are shown as dashed and dotted gray lines, respectively. Figure 4(c) shows the results of the fitting parameters. As for the parameters for $I_2(t)$, A_d increases, and τ_{AM} decreases with increasing fluence, corresponding to the large displacement and stronger damping schematically shown in Fig. 3(b). The relaxation time τ_d does not change noticeably. The small change of f_{AM} is a quite remarkable behavior and a stark difference from the CDW materials of the second-order phase transitions [30,34,40,42,43], where significant changes in f_{AM} as a function of pump fluence have been reported such as the dynamical slowing-down [67] or the overshooting behavior [40]. These observations have been explained in terms of dynamics on the “Mexican-hat” potential in second-order phase transitions. Thus our observation of f_{AM} clearly marks the robust curvature of potential below the threshold in the first-order case [Fig. 4(a)].

As for the parameters for $I_1(t)$, T_s decreases with fluence, and is not equal to the half period (~ 0.3 ps) of the CDW amplitude mode of 1.5 THz. This is in stark contrast to the previous UED work on a Peierls insulator, where the periodic lattice distortion is suppressed on a timescale comparable to half the period of the corresponding collective mode [35]. Afterwards, Hellmann *et al.* performed TARPES measurements on a Peierls insulator and reported that the melting time for the insulating gap was half the period of the CDW amplitude mode [33]. On the other hand, more recent work on $1T\text{-TaS}_2$ reported that the CDW melting time is not equal to half the period of the CDW amplitude mode [41], which is the same conclusion as our current work. With further increasing the fluence to $4.9 \text{ mJ}/\text{cm}^2$, T_s significantly decreases. This behavior is intuitively understood by considering the steeper gradient of the potential with the higher fluence shown in Fig. 4(a). Although the microscopic mechanism determining

the CDW melting time is still elusive, we can stress that it is not simply determined by the CDW amplitude mode. Further considerations of dynamical electron-electron and electron-phonon interactions should be crucial for a deeper understanding, because these intertwined interactions are expected to play an important role especially for materials such as $1T$ -TaS₂ and VTe₂. Lastly, the volume fraction of region 1, r , increases with pump fluence and shows a *threshold-like* behavior at 1.8 mJ/cm² from the linear fits at the low (<1 mJ/cm²) and high fluences (≥ 2.5 mJ/cm²) shown as dashed lines in Fig. 4(c), in close agreement with the value estimated in Fig. 3(c). We show the results at full scale with the errors in Fig. S8 [55]. Much larger values of T_s in the low fluence regime than those in the high fluence regime indicate that the photoinduced phase transition does not completely occur below the threshold fluence.

IV. SUMMARY

In summary, we investigated the CDW amplitude-mode excitations and melting dynamics in VTe₂. The characteristic behaviors of the first-order phase transition were revealed and our work provides valuable insight into the dynamical control of first-order CDW materials. Moreover, the topological surface states controlled via the CDW phase in VTe₂ can be potentially implemented as an ultrafast surface state switching mechanism in technological applications.

ACKNOWLEDGMENTS

This work was supported by Grants-in-Aid for Scientific Research (KAKENHI) (Grants No. JP18K13498, No. JP19H00659, No. JP19H01818, No. JP19H00651, No. JP18K14145, No. JP19H02623, No. JP20H01834, and No. JP21H05235) from the Japan Society for the Promotion of Science (JSPS), by JSPS KAKENHI on Innovative Areas “Quantum Liquid Crystals” (Grant No. JP19H05826), by the Center of Innovation Program from the Japan Science and Technology Agency, JST, the Research and Education Consortium for Innovation of Advanced Integrated Science by JST, and by MEXT Quantum Leap Flagship Program (MEXT Q-LEAP) (Grants No. JPMXS0118067246 and No. JPMXS0118068681), Japan, by a CREST project (No. JP-MJCR20B4). This experiment was performed at BL3 of SACLA with the approval of the Japan Synchrotron Radiation Research Institute (JASRI) (Proposal No. 2022A8024). The synchrotron radiation experiments were performed to evaluate the system at BL19LXU in SPring-8 with the approval of RIKEN (Proposal No. 20220049). The authors would like to acknowledge the support of members of the SACLA and SPring-8 facilities. The authors would like to acknowledge Dr. A. Nakamura for a fruitful discussion. T.S. acknowledges research grants from The Murata Science Foundation, The Hattori Hokokai Foundation, and Toyota Riken Scholar.

-
- [1] H.-H. Kim, S. M. Souliou, M. E. Barber, E. Lefrançois, M. Minola, M. Tortora, R. Heid, N. Nandi, R. A. Borzi, G. Garbarino *et al.*, Uniaxial pressure control of competing orders in a high-temperature superconductor, *Science* **362**, 1040 (2018).
- [2] A. M. Marconnet, M. A. Panzer, and K. E. Goodson, Thermal conduction phenomena in carbon nanotubes and related nanostructured materials, *Rev. Mod. Phys.* **85**, 1295 (2013).
- [3] W. Liao, Y. Huang, H. Wang, and H. Zhang, Van der Waals heterostructures for optoelectronics: Progress and prospects Wu-gang, *Appl. Mater. Today* **16**, 435 (2019).
- [4] Y. Cao, V. Fatemi, S. Fang, K. Watanabe, T. Taniguchi, E. Kaxiras, and P. Jarillo-Herrero, Unconventional superconductivity in magic-angle graphene superlattices, *Nature (London)* **556**, 43 (2018).
- [5] Y. Cao, V. Fatemi, A. Demir, S. Fang, S. L. Tomarken, J. Y. Luo, J. D. Sanchez-Yamagishi, K. Watanabe, T. Taniguchi, E. Kaxiras *et al.*, Correlated insulator behaviour at half-filling in magic-angle graphene superlattices, *Nature (London)* **556**, 80 (2018).
- [6] D. N. Basov, R. D. Averitt, and D. Hsieh, Towards properties on demand in quantum materials, *Nat. Mater.* **16**, 1077 (2017).
- [7] D. Fausti, R. I. Tobey, N. Dean, S. Kaiser, A. Dienst, M. C. Hoffmann, S. Pyon, T. Takayama, H. Takagi, and A. Cavalleri, Light-induced superconductivity in a stripe-ordered cuprate, *Science* **331**, 189 (2011).
- [8] R. Mankowsky, A. Subedi, M. Först, S. O. Mariager, M. Chollet, H. T. Lemke, J. S. Robinson, J. M. Glowina, M. P. Minitti, A. Frano *et al.*, Nonlinear lattice dynamics as a basis for enhanced superconductivity in YBa₂Cu₃O_{6.5}, *Nature (London)* **516**, 71 (2014).
- [9] T. F. Nova, A. S. Disa, M. Fechner, and A. Cavalleri, Metastable ferroelectricity in optically strained SrTiO₃, *Science* **364**, 1075 (2019).
- [10] X. Li, T. Qiu, J. Zhang, E. Baldini, J. Lu, A. M. Rappe, and K. A. Nelson, Terahertz field-induced ferroelectricity in quantum paraelectric SrTiO₃, *Science* **364**, 1079 (2019).
- [11] I. Radu, K. Vahaplar, C. Stamm, T. Kachel, N. Pontius, H. A. Dürr, T. A. Ostler, J. Barker, R. F. L. Evans, R. W. Chantrell *et al.*, Transient ferromagnetic-like state mediating ultrafast reversal of antiferromagnetically coupled spins, *Nature (London)* **472**, 205 (2011).
- [12] P. Roushan, J. Seo, C. V. Parker, Y. S. Hor, D. Hsieh, D. Qian, A. Richardella, M. Z. Hasan, R. J. Cava, and A. Yazdani, Topological surface states protected from backscattering by chiral spin texture, *Nature (London)* **460**, 1106 (2009).
- [13] M. Z. Hasan and C. L. Kane, Topological insulators, *Rev. Mod. Phys.* **82**, 3045 (2010).
- [14] T. Oka and H. Aoki, Photovoltaic Hall effect in graphene, *Phys. Rev. B* **79**, 081406(R) (2009).
- [15] Y. H. Wang, H. Steinberg, P. Jarillo-Herrero, and N. Gedik, Observation of Floquet-Bloch states on the surface of a topological insulator, *Science* **342**, 453 (2013).
- [16] F. Mahmood, C.-K. Chan, Z. Alpichshev, D. Gardner, Y. Lee, P. A. Lee, and N. Gedik, Selective scattering between Floquet-Bloch and Volkov states in a topological insulator, *Nat. Phys.* **12**, 306 (2016).
- [17] J. W. McIver, B. Schulte, F.-U. Stein, T. Matsuyama, G. Jotzu, G. Meier, and A. Cavalleri, Light-induced anomalous Hall effect in graphene, *Nat. Phys.* **16**, 38 (2020).

- [18] E. J. Sie, C. M. Nyby, C. D. Pemmaraju, S. J. Park, X. Shen, J. Yang, M. C. Hoffmann, B. K. Ofori-Okai, R. Li, A. H. Reid *et al.*, An ultrafast symmetry switch in a Weyl semimetal, *Nature (London)* **565**, 61 (2019).
- [19] A. S. Disa, T. F. Nova, and A. Cavalleri, Engineering crystal structures with light, *Nat. Phys.* **17**, 1087 (2021).
- [20] B. Sipos, A. F. Kusmartseva, A. Akrap, H. Berger, L. Forró, and E. Tutiš, From Mott state to superconductivity in $1T$ -TaS₂, *Nat. Mater.* **7**, 960 (2008).
- [21] A. F. Kusmartseva, B. Sipos, H. Berger, L. Forró, and E. Tutiš, Pressure induced superconductivity in pristine $1T$ -TiSe₂, *Phys. Rev. Lett.* **103**, 236401 (2009).
- [22] N. Ru, C. L. Condon, G. Y. Margulis, K. Y. Shin, J. Laverock, S. B. Dugdale, M. F. Toney, and I. R. Fisher, Effect of chemical pressure on the charge density wave transition in rare-earth tritellurides $R\text{Te}_3$, *Phys. Rev. B* **77**, 035114 (2008).
- [23] V. Brouet, W. L. Yang, X. J. Zhou, Z. Hussain, R. G. Moore, R. He, D. H. Lu, Z. X. Shen, J. Laverock, S. B. Dugdale, N. Ru, and I. R. Fisher, Angle-resolved photoemission study of the evolution of band structure and charge density wave properties in $R\text{Te}_3$ ($R=Y, \text{La}, \text{Ce}, \text{Sm}, \text{Gd}, \text{Tb}, \text{and Dy}$), *Phys. Rev. B* **77**, 235104 (2008).
- [24] P. A. Lee and T. M. Rice, Electric field depinning of charge density waves, *Phys. Rev. B* **19**, 3970 (1979).
- [25] D. DiCarlo, E. Sweetland, M. Sutton, J. D. Brock, and R. E. Thorne, Field-induced charge-density-wave deformations and phase slip in NbSe₃, *Phys. Rev. Lett.* **70**, 845 (1993).
- [26] T. L. Adelman, S. V. Zaitsev-Zotov, and R. E. Thorne, Field-effect modulation of charge-density-wave transport in NbSe₃ and TaS₃, *Phys. Rev. Lett.* **74**, 5264 (1995).
- [27] J. Chang, E. Blackburn, O. Ivashko, A. T. Holmes, N. B. Christensen, M. Hücker, R. Liang, D. A. Bonn, W. N. Hardy, U. Rütt, M. v. Zimmermann, E. M. Forgan, and S. M. Hayden, Magnetic field controlled charge density wave coupling in underdoped YBa₂Cu₃O_{6+x}, *Nat. Commun.* **7**, 11494 (2016).
- [28] J. Demsar, K. Biljaković, and D. Mihailovic, Single particle and collective excitations in the one-dimensional charge density wave solid K_{0.3}MoO₃ probed in real time by femtosecond spectroscopy, *Phys. Rev. Lett.* **83**, 800 (1999).
- [29] J. Demsar, L. Forró, H. Berger, and D. Mihailovic, Femtosecond snapshots of gap-forming charge-density-wave correlations in quasi-two-dimensional dichalcogenides $1T$ -TaS₂ and $2H$ -TaSe₂, *Phys. Rev. B* **66**, 041101(R) (2002).
- [30] R. Yusupov, T. Mertelj, V. V. Kabanov, S. Brazovskii, P. Kusar, J.-H. Chu, I. R. Fisher, and D. Mihailovic, Coherent dynamics of macroscopic electronic order through a symmetry breaking transition, *Nat. Phys.* **6**, 681 (2010).
- [31] L. Perfetti, P. A. Loukakos, M. Lisowski, U. Bovensiepen, H. Berger, S. Biermann, P. S. Cornaglia, A. Georges, and M. Wolf, Time evolution of the electronic structure of $1T$ -TaS₂ through the insulator-metal transition, *Phys. Rev. Lett.* **97**, 067402 (2006).
- [32] F. Schmitt, P. S. Kirchmann, U. Bovensiepen, R. G. Moore, L. Rettig, M. Krenz, J.-H. Chu, N. Ru, L. Perfetti, D. H. Lu, M. Wolf, I. R. Fisher, and Z.-X. Shen, Transient electronic structure and melting of a charge density wave in TbTe₃, *Science* **321**, 1649 (2008).
- [33] S. Hellmann, T. Rohwer, M. Kalläne, K. Hanff, C. Sohrt, A. Stange, A. Carr, M. M. Murnane, H. C. Kapteyn, L. Kipp, M. Bauer, and K. Rossnagel, Time-domain classification of charge-density-wave insulators, *Nat. Commun.* **3**, 1069 (2012).
- [34] J. Maklar, Y. W. Windsor, C. W. Nicholson, M. Puppini, P. Walmsley, V. Esposito, M. Porer, J. Rittmann, D. Leuenberger, M. Kubli, M. Savoini, E. Abreu, S. L. Johnson, P. Beaud, G. Ingold, U. Staub, I. R. Fisher, R. Ernstorfer, M. Wolf, and L. Rettig, Nonequilibrium charge-density-wave order beyond the thermal limit, *Nat. Commun.* **12**, 2499 (2021).
- [35] M. Eichberger, H. Schäfer, M. Krumova, M. Beyer, J. Demsar, H. Berger, G. Moriena, G. Sciaini, and R. J. D. Miller, Snapshots of cooperative atomic motions in the optical suppression of charge density waves, *Nature (London)* **468**, 799 (2010).
- [36] N. Erasmus, M. Eichberger, K. Haupt, I. Boshoff, G. Kassier, R. Birmurske, H. Berger, J. Demsar, and H. Schwoerer, Ultrafast dynamics of charge density waves in $4Hb$ -TaSe₂ probed by femtosecond electron diffraction, *Phys. Rev. Lett.* **109**, 167402 (2012).
- [37] K. Haupt, M. Eichberger, N. Erasmus, A. Rohwer, J. Demsar, K. Rossnagel, and H. Schwoerer, Ultrafast metamorphosis of a complex charge-density wave, *Phys. Rev. Lett.* **116**, 016402 (2016).
- [38] A. Kogar, A. Zong, P. E. Dolgirev, X. Shen, J. Straquadine, Y.-Q. Bie, X. Wang, T. Rohwer, I.-C. Tung, Y. Yang, R. Li, J. Yang, S. Weathersby, S. Park, M. E. Kozina, E. J. Sie, H. Wen, P. Jarillo-Herrero, I. R. Fisher, X. Wang *et al.*, Light-induced charge density wave in LaTe₃, *Nat. Phys.* **16**, 159 (2020).
- [39] E. Möhr-Vorobeva, S. L. Johnson, P. Beaud, U. Staub, R. De Souza, C. Milne, G. Ingold, J. Demsar, H. Schaefer, and A. Titov, Nonthermal melting of a charge density wave in TiSe₂, *Phys. Rev. Lett.* **107**, 036403 (2011).
- [40] T. Huber, S. O. Mariager, A. Ferrer, H. Schäfer, J. A. Johnson, S. Grübel, A. Lübcke, L. Huber, T. Kubacka, C. Dornes, C. Laulhe, S. Ravy, G. Ingold, P. Beaud, J. Demsar, and S. L. Johnson, Coherent structural dynamics of a prototypical charge-density-wave-to-metal transition, *Phys. Rev. Lett.* **113**, 026401 (2014).
- [41] C. Laulhé, T. Huber, G. Lantz, A. Ferrer, S. O. Mariager, S. Grübel, J. Rittmann, J. A. Johnson, V. Esposito, A. Lübcke, L. Huber, M. Kubli, M. Savoini, V. L. R. Jacques, L. Cario, B. Corraze, E. Janod, G. Ingold, P. Beaud, S. L. Johnson *et al.*, Ultrafast formation of a charge density wave state in $1T$ -TaS₂: Observation at nanometer scales using time-resolved x-ray diffraction, *Phys. Rev. Lett.* **118**, 247401 (2017).
- [42] M. Trigo, P. Giraldo-Gallo, M. E. Kozina, T. Henighan, M. P. Jiang, H. Liu, J. N. Clark, M. Chollet, J. M. Glowina, D. Zhu, T. Katayama, D. Leuenberger, P. S. Kirchmann, I. R. Fisher, Z. X. Shen, and D. A. Reis, Coherent order parameter dynamics in SmTe₃, *Phys. Rev. B* **99**, 104111 (2019).
- [43] M. Burian, M. Porer, J. R. L. Mardegan, V. Esposito, S. Parchenko, B. Burganov, N. Gurung, M. Ramakrishnan, V. Scagnoli, H. Ueda, S. Francoal, F. Fabrizi, Y. Tanaka, T. Togashi, Y. Kubota, M. Yabashi, K. Rossnagel, S. L. Johnson, and U. Staub, Structural involvement in the melting of the charge density wave in $1T$ -TiSe₂, *Phys. Rev. Res.* **3**, 013128 (2021).
- [44] A. J. Sternbach, F. L. Ruta, Y. Shi, T. Slusar, J. Schalch, G. Duan, A. S. McLeod, X. Zhang, M. Liu, A. J. Millis, H.-T. Kim, L.-Q. Chen, R. D. Averitt, and D. N. Basov, Nanotextured

- dynamics of a light-induced phase transition in VO₂, *Nano Lett.* **21**, 9052 (2021).
- [45] S. W. Teitelbaum, B. K. Ofori-Okai, Y.-H. Cheng, J. Zhang, F. Jin, W. Wu, R. D. Averitt, and K. A. Nelson, Dynamics of a persistent insulator-to-metal transition in strained manganese films, *Phys. Rev. Lett.* **123**, 267201 (2019).
- [46] K. D. Bronsema, G. W. Bus, and G. A. Wiegers, The crystal structure of vanadium ditelluride, V_{1+x}Te₂, *J. Solid State Chem.* **53**, 415 (1984).
- [47] R. Brouwer and F. Jellinek, The low temperature superstructures of 1T-TaSe₂ and 2H-TaSe₂, *Physica B+C* **99**, 51 (1980).
- [48] T. Ohtani, K. Hayashi, M. Nakahira, and H. Nozaki, Phase transition in V_{1+x}Te₂ (0.04 ≤ x ≤ 0.11), *Solid State Commun.* **40**, 629 (1981).
- [49] N. Mitsuishi, Y. Sugita, M. S. Bahramy, M. Kamitani, T. Sonobe, M. Sakano, T. Shimojima, H. Takahashi, H. Sakai, K. Horiba, H. Kumigashira, K. Taguchi, K. Miyamoto, T. Okuda, S. Ishiwata, Y. Motome, and K. Ishizaka, Switching of band inversion and topological surface states by charge density wave, *Nat. Commun.* **11**, 2466 (2020).
- [50] A. Nakamura, T. Shimojima, M. Matsuura, Y. Chiashi, M. Kamitani, H. Sakai, S. Ishiwata, H. Li, A. Oshiyama, and K. Ishizaka, Evaluation of photo-induced shear strain in monoclinic VTe₂ by ultrafast electron diffraction, *Appl. Phys. Express* **11**, 092601 (2018).
- [51] A. Nakamura, T. Shimojima, Y. Chiashi, M. Kamitani, H. Sakai, S. Ishiwata, H. Li, and K. Ishizaka, Nanoscale imaging of unusual photoacoustic waves in thin flake VTe₂, *Nano Lett.* **20**, 4932 (2020).
- [52] H. Tanimura, N. L. Okamoto, T. Homma, Y. Sato, A. Ishii, H. Takamura, and T. Ichitsubo, Nonthermal melting of charge density wave order via nucleation in VTe₂, *Phys. Rev. B* **105**, 245402 (2022).
- [53] M. Tuniz, D. Soranzio, D. Bidoggia, D. Puntel, W. Bronsch, S. L. Johnson, M. Peressi, F. Parmigiani, and F. Cilento, Ultrafast all-optical manipulation of the charge-density-wave in VTe₂, *arXiv:2305.03528*.
- [54] T. Ishikawa, H. Aoyagi, T. Asaka, Y. Asano, N. Azumi, T. Bizen, H. Ego, K. Fukami, T. Fukui, Y. Furukawa *et al.*, A compact x-ray free-electron laser emitting in the sub-ångström region, *Nat. Photon.* **6**, 540 (2012).
- [55] See Supplemental Material at <http://link.aps.org/supplemental/10.1103/PhysRevB.108.184305> for details of the experimental setup and bulk sample preparation, flake sample preparation, estimation of the sample thickness, lattice vectors and Bragg reflection index, calculations of structure factors, and the results of the fitting parameters in full scale, which includes Refs. [56–61].
- [56] T. Togashi, S. Owada, Y. Kubota, K. Sueda, T. Katayama, H. Tomizawa, T. Yabuuchi, K. Tono, and M. Yabashi, Femtosecond optical laser system with spatiotemporal stabilization for pump-probe experiments at SACLA, *Appl. Sci.* **10**, 7934 (2020).
- [57] M. Yabashi, H. Tanaka, and T. Ishikawa, Overview of the SACLA facility, *J. Synchrotron Radiat.* **22**, 477 (2015).
- [58] T. Kameshima, S. Ono, T. Kudo, K. Ozaki, Y. Kirihara, K. Kobayashi, Y. Inubushi, M. Yabashi, T. Horigome, A. Holland, K. Holland, D. Burt, H. Murao, and T. Hatsui, Development of an x-ray pixel detector with multi-port charge-coupled device for x-ray free-electron laser experiments, *Rev. Sci. Instrum.* **85**, 033110 (2014).
- [59] M. Onodera, S. Masubuchi, R. Moriya, and T. Machida, Assembly of van der Waals heterostructures: Exfoliation, searching, and stacking of 2D materials, *Jpn. J. Appl. Phys.* **59**, 010101 (2020).
- [60] *International Tables for Crystallography, Volume C: Mathematical, Physical and Chemical Tables*, edited by E. Prince (Wiley, Hoboken, NJ, 2004).
- [61] <https://dx.doi.org/10.18434/T4HS32>.
- [62] T. Suzuki, Y. Kubota, A. Nakamura, T. Shimojima, K. Takubo, S. Ito, K. Yamamoto, S. Michimae, H. Sato, H. Hiramatsu, H. Hosono, T. Togashi, M. Yabashi, H. Wadati, I. Matsuda, S. Shin, and K. Okazaki, Ultrafast optical stress on BaFe₂As₂, *Phys. Rev. Res.* **3**, 033222 (2021).
- [63] A. W. Overhauser, Observability of charge-density waves by neutron diffraction, *Phys. Rev. B* **3**, 3173 (1971).
- [64] H. J. Zeiger, J. Vidal, T. K. Cheng, E. P. Ippen, G. Dresselhaus, and M. S. Dresselhaus, Theory for dispersive excitation of coherent phonons, *Phys. Rev. B* **45**, 768 (1992).
- [65] K. Binder, Theory of first-order phase transitions, *Rep. Prog. Phys.* **50**, 783 (1987).
- [66] H. Ichikawa, S. Nozawa, T. Sato, A. Tomita, K. Ichianagi, M. Chollet, L. Guerin, N. Dean, A. Cavalleri, S. Adachi, T. Arima, H. Sawa, Y. Ogimoto, M. Nakamura, R. Tamaki, K. Miyano, and S. Koshihara, Transient photoinduced “hidden” phase in a manganite, *Nat. Mater.* **10**, 101 (2011).
- [67] A. Zong, P. E. Dolgirev, A. Kogar, E. Ergecen, M. B. Yilmaz, Y.-Q. Bie, T. Rohwer, I-Cheng Tung, J. Straquadine, X. Wang, Y. Yang, X. Shen, R. Li, J. Yang, S. Park, M. C. Hoffmann, B. K. Ofori-Okai, M. E. Kozina, H. Wen, X. Wang, I. R. Fisher *et al.*, Dynamical slowing-down in an ultrafast photoinduced phase transition, *Phys. Rev. Lett.* **123**, 097601 (2019).